The Astrophysical Journal Supplement Series, 241:13 (9pp), 2019 March https://doi.org/10.3847/1538-4365/ab041e

New Spectral Characterization of Dimethyl Ether Isotopologues CH_3OCH_3 and $^{13}CH_3OCH_3$ in the THz Region

J. M. Fernández[1], G. Tejeda[1], M. Carvajal[2,3], and M. L. Senent[4]
[1] Laboratory of Molecular Fluid Dynamics, Instituto de Estructura de la Materia IEM-CSIC, Unidad Asociada GIFMAN, CSIC-UHU; E-28006 Madrid, Spain
jm.fernandez@csic.es
[2] Dpto. Ciencias Integradas, Centro de Estudios Avanzados en Física, Matemática y Computación, Facultad de Ciencias Experimentales, Universidad de Huelva; Unidad Asociada GIFMAN, CSIC-UHU; E-21071 Huelva, Spain
[3] Instituto Universitario Carlos I de Física Teórica y Computacional, Universidad de Granada, Granada, Spain
[4] Theoretical Chemistry and Physics Department, Instituto de Estructura de la Materia IEM-CSIC, Unidad Asociada GIFMAN, CSIC-UHU; E-28006 Madrid, Spain
Received 2018 November 27; revised 2019 January 24; accepted 2019 February 1; published 2019 March 14

Abstract

The torsional Raman spectra of two astrophysically detected isotopologues of dimethyl ether (DME, $^{12}CH_3O^{12}CH_3$ and $^{13}CH_3O^{12}CH_3$) have been recorded at room temperature and cooled in a supersonic jet and interpreted with the help of highly correlated ab initio calculations. DME displays excited torsional and vibrational levels at low energy that can be populated at the temperatures of the star-forming regions, obliging to extend the analysis of the rotational spectrum over the ground state. Its spectrum in the THz region is rather complex due to the coupling of the torsional overtones $2\nu_{11}$ and $2\nu_{15}$ with the COC-bending mode and the presence of many hot bands. The torsional overtones are set here at $2\nu_{11} = 385.2$ cm^{-1} and $2\nu_{15} = 482.0$ cm^{-1} for $^{12}CH_3O^{12}CH_3$ and $2\nu_{11} = 385.0$ cm^{-1} and $2\nu_{15} = 481.1$ cm^{-1} for $^{13}CH_3O^{12}CH_3$. The new assignment of $2\nu_{11}$ is downshifted around $\sim$10 cm^{-1} with respect to the literature. All the other (hot) bands have been reassigned consistently. In addition, the infrared-forbidden torsional fundamental band ν_{11} is observed here at 197.8 cm^{-1}. The new spectral characterization in the THz region reported here provides improved values of the Hamiltonian parameters to be used in the analysis of the rotational spectra of DME isotopologues for further astrophysical detections.

Key words: astrochemistry – ISM: lines and bands – ISM: molecules – methods: laboratory: molecular – molecular data – techniques: spectroscopic

1. Introduction

Dimethyl ether (DME, CH_3OCH_3) is a relevant astrophysical molecule that was first detected in the interstellar medium (ISM) by Snyder et al. (1974) and later on was identified as an abundant species in star-forming regions (Schilke et al. 2001). DME is mainly formed in the gas phase via the radiative association reaction of methoxy and methyl radicals, and it presents a correlation with methyl formate (Carvajal et al. 2010; Favre et al. 2014), via the oxidation of CH_3OCH_2, in cold objects (Balucani et al. 2015).

In addition to works prior to its detection in the ISM (Taylor & Vidale 1957; Kasai & Myers 1959; Fateley & Miller 1962; Blukis et al. 1963; Durig et al. 1976; Groner & Durig 1977), the astrophysical interest for the complete description of the spectrum in the millimeter and submillimeter regions of DME and its isotopologues, such as $^{13}CH_3OCH_3$ (^{13}C-DME) and CH_3OCH_2D (d-DME), has brought about many laboratory studies of its rotational spectrum and of a few vibrational bands (Lovas et al. 1979; Neustock et al. 1990; Groner et al. 1998; Coudert et al. 2002; Niide & Hayashi 2003; Endres et al. 2009; Kutzer et al. 2016). In turn, the analysis of an extensive number of spectral lines in astronomical observations has given rise to the identification of DME in Orion-KL (Brouillet et al. 2013) and the detection of the first excited torsional states lines in a high-mass star-forming region (Bisschop et al. 2013). Furthermore, the ground state rotational lines corresponding to the monosubstituted isotopologues ^{13}C-DME and d-DME were first observed in a high-mass star-forming region (Koerber et al. 2013; Richard et al. 2013).

DME is a nonrigid asymmetric top with two methyl internal rotors that splits each rovibrational level into nine components (Groner & Durig 1977; Senent et al. 1995a, 1995b), some of them degenerate. Hence, the high-resolution spectrum of DME is quite dense, and its analysis is challenging. Furthermore, because the first and the second excited torsional levels lie at relatively low energy, they can be populated at the temperatures of the hot core regions, obliging to extend the spectral analysis to the two torsional fundamentals and their overtones. The spectral region of the torsional overtones is further complicated due to their coupling with the COC-bending mode (Senent et al. 1995b) and the presence of many hot bands. The following notation will be used throughout the paper: ν_{11} is the "anti-geared" torsion, ν_{15} is the "geared" torsion, and ν_7 is the COC-bending mode; vib-torsional energy levels will be denoted as (v_{11} v_{15} v_7), where v_n is the number of torsional or vibrational quanta in the corresponding mode.

The torsional spectrum of DME was investigated experimentally at room temperature by Groner & Durig (1977), using Raman and infrared techniques. The torsional fundamental ν_{15} was observed at 241.0 cm^{-1}. The other torsional fundamental ν_{11} is forbidden in the absorption spectrum and was estimated between 199 and 202 cm^{-1}. The two torsional overtones were assigned to the peaks observed at $2\nu_{11} = 395.5$ cm^{-1} and $2\nu_{15} = 481.2$ cm^{-1}. The lack of an accurate value for the ν_{11} torsional mode prevented the determination of some of the interaction parameters of the effective Hamiltonian needed for a further analysis.

In this paper, the torsional Raman spectra of DME and of ^{13}C-DME have been recorded at room temperature and of cooled DME in a supersonic jet. The spectrum of cooled DME allowed us to assign unequivocally the torsional overtones and their first hot bands, amending some of the previous assignments. In turn,

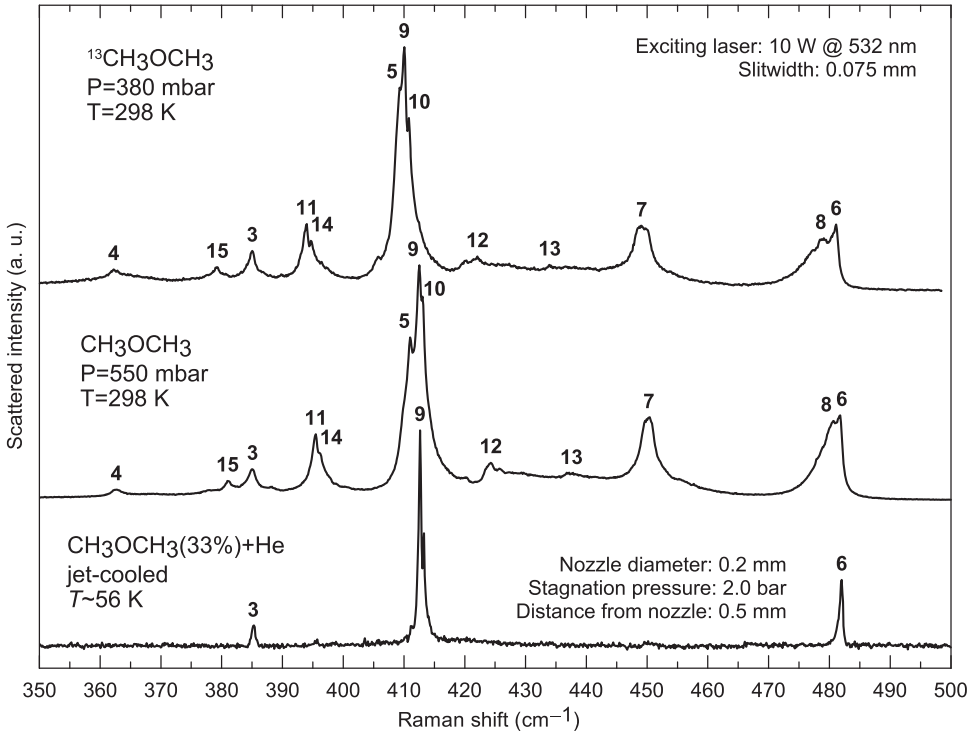

Figure 1. Raman spectra of CH_3OCH_3 and $^{13}CH_3OCH_3$ in the region of the torsional overtones. For band numbering, refer to Table 2.

the new frequencies have been used to refine 3D quantum calculations, employing a state-of-the-art coupled-cluster theory with single and double substitutions (CCSD(T)) ab initio calculations (Villa et al. 2011) and a torsion–torsion-bending Hamiltonian (Senent et al. 1995b; Carvajal et al. 2012). The new characterization provides improved values of the Hamiltonian parameters for the analysis of DME and ^{13}C-DME rotational spectra and future astrophysical detections.

2. New Experimental Raman Measurements

Two sets of Raman spectra of DME were recorded in this work: (i) at room temperature and (ii) jet cooled. The sample of DME was supplied by Praxair, with nominal purity of 99.8%, while that of ^{13}C-DME was synthesized in the University of Kassel, Germany (Kutzer et al. 2016); the latter sample was distilled by liquid nitrogen to remove residual H_2 from the synthesis. Raman spectra of DME and of ^{13}C-DME were recorded at room temperature under static conditions (pressure 550 mbar and 380 mbar, respectively). In addition, supersonic jets of mixtures of DME diluted in He were produced to cool the DME. Raman shifts were calibrated against Hg and Ne emission lines and are accurate to ± 0.1 cm^{-1}. Raman scattering was excited by 10 W of linearly polarized radiation at 532 nm from a Coherent Verdi V10 laser, which was sharply focused down to a 15 μm beam waist on the sample by a $f = 35$ mm lens. Scattered radiation perpendicular to both laser propagation and polarization was collected by an $f = 55$ mm photographic objective (Nikon, $f/1.8$) and projected, with a total magnification $\times 10$, onto the entrance slit of the spectrograph. This is a Jobin-Yvon double monochromator, equipped with two 2400 groove/mm gratings, and a CCD detector with 13×13 μm^2 pixels, which is refrigerated by liquid nitrogen. The entrance slit was 75 and 150 μm, yielding a spectral resolution of 0.36 and 0.72 cm^{-1}, respectively. Several scans were spike filtered and averaged.

Raman spectroscopy can be an invaluable tool to investigate the torsional modes of symmetric molecules like ethane (Fantoni et al. 1986; Fernández-Sánchez et al. 1989), propane (Engeln et al. 1990), or butane (Compton et al. 1980; Engeln & Reuss 1991). In such symmetric molecules, some of the torsional modes are forbidden in infrared (IR) or microwave (MW) absorption, while the torsional overtones give rise to weak Q-branches in Raman spectrum, often accompanied by a rich structure of hot bands. In the case of DME, the ν_{11} torsional mode is silent in IR–MW; on the contrary, the two torsional modes are Raman allowed, as well as their overtones. The Raman spectra of DME and ^{13}C-DME in this latter region are shown in Figure 1. This region is dominated by the COC-bending mode ν_7, which yields the peak at $\sim$410 cm^{-1}. In addition to that, a rich structure of peaks due to hot bands can be seen, what hinders the safe assignment of the two torsional overtones. The spectrum of ^{13}C-DME is rather similar to that of DME, with some of the peaks shifted toward lower wavenumbers, due to the mass increase, as discussed below. The lowest panel shows the spectrum of jet-cooled DME in a supersonic expansion diluted in helium. As can be clearly seen, only three peaks survive at low temperature, which can be assigned unambiguously to the two torsional overtones plus the COC-bending modes. Actually, the $2\nu_{11}$ torsional overtone had been wrongly assigned (Groner & Durig 1977) to the peak at 395.5 cm^{-1} in the room temperature spectrum, which disappears when the molecule is jet cooled, while the peak at 385.2 cm^{-1} remains at low temperature.

The Raman spectrum of the jet-cooled DME in the region of the torsional fundamentals is shown in Figure 2. These Raman bands are extremely weak and had not been reported before. The faint Q branch at 241.4 cm^{-1} is the ν_{15} mode, which was observed previously in IR (Fateley & Miller 1962; Groner & Durig 1977). The broad band with the comb-like rotational structure can be assigned to the unobserved ν_{11} torsional

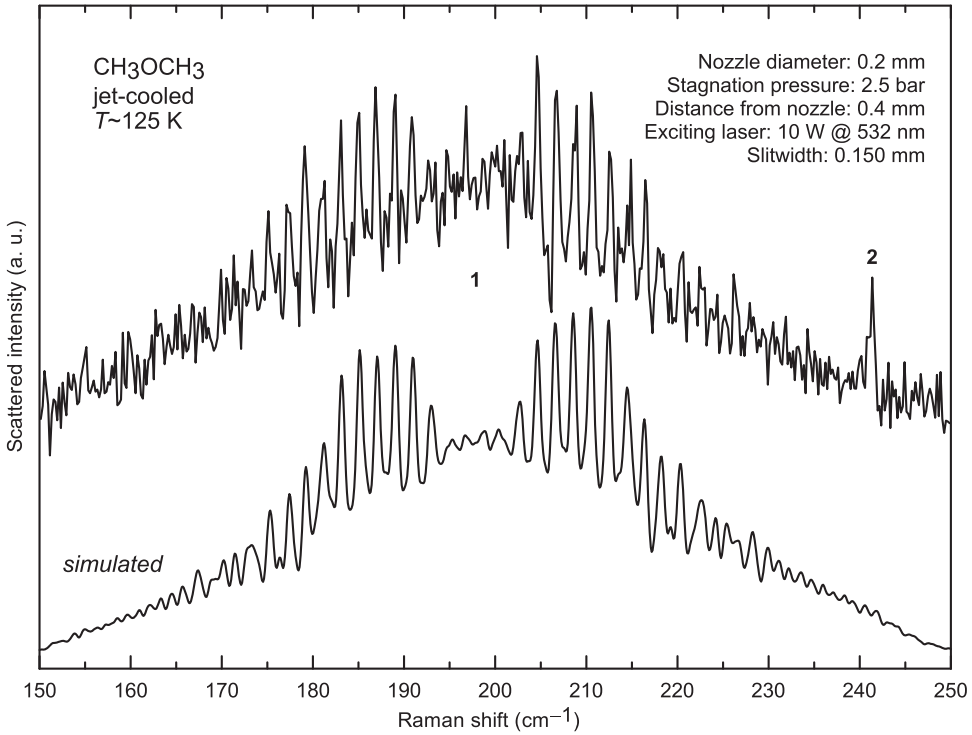

Figure 2. Raman spectrum of jet-cooled CH_3OCH_3 in the region of the torsional fundamentals. For band numbering, refer to Table 2.

fundamental. A simulation with PGOPHER (Western 2016), with the selection rules $\Delta K_a = \pm 1$ and $\Delta K_c = \pm 1$, corresponding to a Raman band of A_2 symmetry in the C_{2v} point group, allows us to locate the band origin at 197.8 cm^{-1}, although it could be downshifted by one unit of the peak spacing (1.9 cm^{-1}).

3. Theoretical Model for the Spectral Analysis

In previous papers on DME (Villa et al. 2011) and its isotopologues CH_3OCD_3, CD_3OCD_3 (Senent et al. 2012), $^{13}CH_3OCH_3$ (Carvajal et al. 2012), and CH_3OCH_2D (Carvajal et al. 2014), we used a 3D model for the analysis of their far-IR spectra. Assuming that the three low-frequency vibrational modes can be treated separately from the remaining "high-frequency" vibrations, the 3D Hamiltonian can be written as

$$\hat{H}(\alpha, \theta_1, \theta_2) = -\sum_{i=1}^{3}\sum_{j=1}^{3}\frac{\partial}{\partial q_i}B_{ij}(\alpha, \theta_1, \theta_2)\frac{\partial}{\partial q_j} + V^{\text{eff}}(\alpha, \theta_1, \theta_2). \quad (1)$$

In this equation, q_i, $q_j = (\alpha, \theta_1, \theta_2)$ represent the three independent variables: the COC-bending α and the two torsional coordinates, θ_1 and θ_2. The first term, which depends on the B_{ij} parameters (the G-matrix elements in cm^{-1}), is a 3D-kinetic energy operator. The second term, the effective potential energy V^{eff}, is the sum of three contributions:

$$V^{\text{eff}}(\alpha, \theta_1, \theta_2) = V(\alpha, \theta_1, \theta_2) + V'(\alpha, \theta_1, \theta_2) + V^{\text{ZPVE}}(\alpha, \theta_1, \theta_2) \quad (2)$$

where $V(\alpha, \theta_1, \theta_2)$ is the ab initio potential energy, $V'(\alpha, \theta_1, \theta_2)$ is the Podolsky pseudopotential, and $V^{\text{ZPVE}}(\alpha, \theta_1, \theta_2)$ is the zero-point vibrational energy correction. The ab initio potential energy V is isotopically invariant, whereas V' and V^{ZPVE} (and thus the effective potential V^{eff}) depend on the nuclear masses, as well as, of course, the kinetic energy parameters B_{ij}.

All of the terms in Equations (1) and (2) can be determined from energies, geometries, and harmonic frequencies from accurate ab initio calculations, as described elsewhere (Senent 1998a, 1998b). In the present paper, we used the previous ab initio calculations by Villa et al. (2011), performed with the Gaussian 09 code (Frisch et al. 2009). CCSD (Scuseria & Schaefer 1989) was employed for the geometry optimizations. To improve the energies, single point calculations were performed, adding a perturbative treatment of triple excitations (CCSD(T); Pople et al. 1987) on the CCSD geometries. Long range effects are well described because the augmented aug-cc-pVTZ basis set was employed in all of the computations (Woon & Dunning 1993).

Ab initio energies $V(\alpha, \theta_1, \theta_2)$ were calculated at 126 configurations for selected values of the three $(\alpha, \theta_1, \theta_2)$ coordinates: $\alpha = (104.^{\circ}676 \rightarrow 119.^{\circ}676, \Delta\alpha = 3^{\circ})$, and θ_1, $\theta_2 = 0^{\circ}, \pm 30^{\circ}, \pm 90^{\circ}, \pm 150^{\circ}, 180^{\circ}$. In all of the 126 configurations, the remaining $3N - 9$ internal coordinates were allowed to relax. The other terms of the Hamiltonian, B_{ij}, V', and V^{ZPVE}, were also computed for the same 126 configurations; the V^{ZPVE} correction, which was needed to obtain reliable results (Smeyers et al. 1996), was computed within the harmonic approximation. Analytical 3D effective potential energy surfaces $V^{\text{eff}}(\alpha, \theta_1, \theta_2)$ for DME and ^{13}C-DME were then obtained by fitting their values at the 126 configurations to a series of the form:

$$V^{\text{eff}}(\alpha, \theta_1, \theta_2) = \sum_{l=0}^{3}\left[\sum_{m=0}^{2}\sum_{n=0}^{2}A_{lmn}\,\alpha^l\cos(3m\theta_1)\cos(3n\theta_2) + B_{l11}\alpha^l\sin(3\theta_1)\sin(3\theta_2)\right]. \quad (3)$$

For DME, $A_{lmn} = A_{lnm}$ and $B_{lmn} = B_{lnm}$, while for the less symmetric ^{13}C-DME, the $|A_{lmn} - A_{lnm}|$, and $|B_{lmn} - B_{lnm}|$

differences are found to be lower than 0.0001 cm^{-1}. Formally identical fits were carried out for each of the kinetic energy operators $B_{ij}(\alpha, \theta_1, \theta_2)$.

The original code ENEDIM (Senent 2001) was used to carry out the calculations and fits of the $V^{eff}(\alpha, \theta_1, \theta_2)$ and $B_{ij}(\alpha, \theta_1, \theta_2)$ surfaces and then to compute variationally the torsional and bending energy levels of the 3D Hamiltonian. To reduce the computational expenses and for the classification of the levels, the molecular symmetry properties were taken into consideration. The two isotopologues studied here, $^{12}CH_3O^{12}CH_3$ (DME) and $^{13}CH_3O^{12}CH_3$ (^{13}C-DME), can be classified in the G_{36} and G_{18} Molecular Symmetry Groups (Bunker & Jensen 1989), respectively. G_{36} contains nine irreducible representations: four nondegenerate A_1, A_2, A_3, and A_4, four doubly-degenerate E_1, E_2, E_3, and E_4 and one four-fold degenerate G. G_{18} contains two nondegenerate representations, A_1 and A_2, and four double-degenerate ones, E_1, E_2, E_3, and E_4. The correlation between G_{36} and G_{18} representations was detailed previously (Carvajal et al. 2012; Villa et al. 2013).

In our previous papers (Villa et al. 2011; Carvajal et al. 2014), the parameters of the ab initio Hamiltonian were refined to reproduce the old available experimental frequencies of Groner & Durig (1977). In the present work, the refinement has been revisited (see Table 1) using the new Raman observations, as described in the next section. We can anticipate that the ab initio calculations are closer to the new experimental data than to the old ones.

4. Discussion

The new Raman spectra of cooled DME reported here (see Figures 1 and 2) were crucial for the right assignment of the torsional modes and their overtones. At $T = 56$ K, only three bands survive in the recorded Raman spectrum of DME in the bottom trace of Figure 1. At such a low T, only transitions starting from the ground state (000) can be observed, due to the population distribution. Thus, the observed three peaks can be safely assigned to the transitions from ground state to the (200), (001), and (020) levels, respectively. This has allowed us to reassign the torsional overtone (200) and, with the help of the ab initio calculations, to amend the assignment of other bands already reported in both IR and Raman spectra. In fact, Groner & Durig (1977) proposed that the torsional overtone (200) of DME lie at 395.5 cm^{-1} and its first hot band (100) → (300) at 385.0 cm^{-1} whereas, in this work, they are set at 385.2 cm^{-1} and 362.6 cm^{-1}, respectively. These new assignments are downshifted by around ∼10 cm^{-1} and ∼22 cm^{-1} with respect to those by Groner & Durig (1977). The peak around 395 cm^{-1} is assigned here to two overlapping hot bands of the ν_7 bending: (010) → (011) and (001) → (002). The remaining prominent feature at ∼450 cm^{-1} in Figure 1, unassigned in Groner & Durig (1977), is the hot band (100) → (120).

The complete lists of the experimental wavenumbers for both DME and ^{13}C-DME, along with their assignments and calculated torsional splittings, are displayed in Table 2. The accuracy of the reported wavenumbers is mainly determined by the line shape, as a result of the (unresolved) rotational structure and/or torsional splittings. Thus, the quoted uncertainties range from ±0.2 cm^{-1} for isolated narrow bands up to ±0.5 cm^{-1} for broad, overlapped, or weak bands. As a representative check, the (001) bending energy levels, observed here at 412.5 cm^{-1} for DME and 410.0 cm^{-1} for ^{13}C-DME, are consistent within the experimental error with the more accurate values (412.350 and 409.993 cm^{-1}) reported recently by Kutzer et al. (2016).

It is worth discussing the isotopic shifts, from DME to ^{13}C-DME, of the peaks in Figure 1 in light of this new assignment. The larger isotopic shifts (∼2.5 cm^{-1}) are those of the COC-bending mode (and their overtones and combinations), which are directly affected by the increased mass of one of the C atoms. On the contrary, in zeroth-order approximation, the torsional modes (due to the internal rotation of the two methyl groups) should not be affected by the mass of the C atoms because they lie on the rotation axis and thus do not contribute to the rotor moment of inertia. Of course, coupling between the bending and the torsional modes leads to the observed isotopic shifts of the torsional overtones. The ν_{15} mode is more strongly coupled to the bending of the COC skeletal frame (as revealed by its higher frequency and intensity) than the ν_{11} mode. Thus, the new assignment proposed here is further supported by the tiny isotopic shift (0.2–0.4 cm^{-1}) of the peaks involving ν_{11}, as opposed to those (∼1 cm^{-1}) involving ν_{15}.

To obtain the best fit parameters of the effective Hamiltonian, we started from the ab initio potential energy surfaces and the ab initio kinetic parameters calculated in our previous works on DME (Villa et al. 2011) and ^{13}C-DME (Carvajal et al. 2012). Those ab initio calculations provided a reasonable description of the torsional features but failed to reproduce the bending fundamental ν_7 (421.64 cm^{-1} ab initio versus 412.35 cm^{-1}, as observed by Kutzer et al. 2016). The ab initio Hamiltonian was then refined in this work following three steps: (i) the adjustment of the bending fundamental close to the experimental value, (ii) the reassignment of the two torsional fundamentals and their overtones according to the new Raman spectra, and (iii) the assignment of the other observed bands and the subsequent global fit of the Hamiltonian. The main difference between the old Hamiltonians from Villa et al. (2011) and Carvajal et al. (2012) and the present one involves the second step. These three steps are detailed next.

(i) The main weakness of the ab initio potential energy surface (Villa et al. 2011) concerns the employed definition of the COC-bending coordinate, which was set to the COC angle α, missing the contribution of other coordinates, such as the in-plane HCO angles. Therefore, for a more realistic description of the COC bending, a new α' coordinate was introduced:

$$\alpha' = \alpha\,(1 + F/100), \tag{4}$$

where F is a factor that corrects the contribution of the curvilinear internal coordinate angle to the normal COC-bending coordinate. Hence, the $B_{\alpha,\alpha}$ kinetic parameter was also corrected in all of the conformations. For DME and ^{13}C-DME, F was optimized to be 1.954 (Villa et al. 2011; Carvajal et al. 2012) to reproduce the experimental bending energy term values. This represents a coordinate correction lower than 2%.

(ii) The ab initio torsional overtones of DME (Villa et al. 2011), when compared with the experimental data by Groner & Durig (1977), yielded the differences (obs-calc) $\Delta = 395.5 - 388.61 = +6.89$ cm^{-1} for $2\nu_{11}$ and $\Delta = 481.2 - 487.22 = -6.02$ cm^{-1} for $2\nu_{15}$. One torsional overtone seemed to be underestimated by the calculations whereas the other one appeared overestimated. In the subsequent adjustment (Villa et al. 2011), the potential term B_{011} in Equation (3), one of the main responsible for the gap between

Table 1
Energies (in cm^{-1}) of the Lowest Torsional and Bending Levels of DME and ^{13}C-DME

(v_{11} v_{15} v_7)	Symm.	$^{12}CH_3O^{12}CH_3$		Symm.	$^{13}CH_3O^{12}CH_3$	
		OLD[a]	NEW[b]		OLD[c]	NEW[b]
0 0 0	A1	0.000	0.000	A1	0.000	0.000
	G	0.000	0.000	E1	0.000	0.000
	E1	0.001	0.001	E2	0.000	0.000
	E3	0.001	0.001	E3	0.001	0.001
				E4	0.001	0.001
1 0 0	A3	201.611	198.341	A2	200.912	197.359
	G	201.602	198.332	E1	200.903	197.350
	E2	201.593	198.323	E2	200.904	197.350
	E3	201.593	198.323	E3	200.895	197.341
				E4	200.895	197.341
0 1 0	A2	241.783	242.603	A2	241.607	242.686
	G	241.774	242.593	E1	241.598	242.676
	E1	241.765	242.584	E2	241.598	242.676
	E4	241.765	242.584	E3	241.589	242.667
				E4	241.589	242.667
2 0 0	A1	391.094	386.528	A1	389.609	384.831
	G	391.225	386.658	E1	389.732	384.954
	E1	391.358	386.789	E2	389.734	384.956
	E3	391.358	386.789	E3	389.859	385.081
				E4	389.859	385.081
0 0 1	A1	412.086	413.042	A1	409.170	410.432
	G	412.086	413.039	E1	409.173	410.430
	E1	412.087	413.036	E2	409.173	410.430
	E3	412.087	413.036	E3	409.176	410.428
				E4	409.176	410.428
1 1 0	A4	422.176	420.471	A1	421.629	419.905
	G	422.393	420.691	E1	421.846	420.123
	E2	422.609	420.910	E2	421.838	420.116
	E4	422.609	420.910	E3	422.053	420.333
				E4	422.054	420.333
0 2 0	A1	480.889	481.940	A1	479.987	481.654
	G	480.960	482.020	E1	480.059	481.734
	E1	481.031	482.099	E2	480.057	481.731
	E3	481.031	482.099	E3	480.129	481.811
				E4	480.129	481.811
3 0 0	A3	569.642	564.130	A2	568.029	562.043
	G	567.967	562.616	E1	566.480	560.650
	E2	566.614	561.352	E2	566.406	560.592
	E3	566.615	561.352	E3	565.143	559.416
				E4	565.143	559.416
2 1 0	A2	590.656	587.974	A2	589.896	587.047
	G	588.364	585.674	E1	587.584	584.752
	E1	585.795	583.182	E2	587.703	584.850
	E4	585.797	583.184	E3	585.152	582.397
				E4	585.153	582.398
1 0 1	A3	613.117	611.569	A2	610.202	608.235
	G	613.206	611.610	E1	610.290	608.283
	E2	613.294	611.643	E2	610.291	608.286
	E3	613.294	611.642	E3	610.379	608.329
				E4	610.378	608.329
0 1 1	A2	636.395	638.255	A2	634.044	636.816
	G	636.449	638.313	E1	634.095	636.870
	E1	636.506	638.371	E2	634.090	636.867
	E4	636.507	638.372	E3	634.144	636.922
				E4	634.144	636.923
1 2 0	A3	648.652	647.438	A2	646.719	645.721

Table 1
(Continued)

(v_{11} v_{15} v_7)	Symm.	$^{12}CH_3O^{12}CH_3$		Symm.	$^{13}CH_3O^{12}CH_3$	
		OLD[a]	NEW[b]		OLD[c]	NEW[b]
	G	647.493	646.185	E1	645.527	644.432
	E2	646.295	644.894	E2	645.564	644.471
	E3	646.286	644.884	E3	644.328	643.140
				E4	644.319	643.129
4 0 0	A1	706.250	703.223	A1	705.812	702.388
	G	708.488	705.787	E1	707.928	704.883
	E1	727.268	723.674	E2	708.391	705.332
	E3	726.577	722.224	E3	726.116	722.212
				E4	725.509	720.574
0 3 0	A2	717.917	718.784	A2	716.038	718.141
	G	717.442	718.122	E1	715.594	717.483
	E1	716.716	716.717	E2	715.601	717.481
	E4	717.059	717.671	E3	714.923	715.883
				E4	715.225	717.040
3 1 0	A4	711.733	709.884	A1	711.676	709.692
	G	731.779	728.819	E1	731.382	728.093
	E2	735.657	733.397	E2	730.719	727.475
	E4	736.031	733.928	E3	735.199	732.699
				E4	735.531	733.219
2 2 0	A1	785.149	779.346	A1	783.614	777.555
	G	784.508	779.640	E1	783.133	778.089
	E1	783.988	779.822	E2	783.084	778.032
	E3	783.912	779.724	E3	782.666	778.371
				E4	782.595	778.274
0 0 2	A1	805.550	806.600	A1	800.434	802.112
	G	805.861	806.826	E1	800.978	802.594
	E1	806.194	807.097	E2	800.964	802.564
	E3	806.105	806.966	E3	801.516	803.083
				E4	801.443	802.962
1 3 0	A4	810.976	810.464	A1	809.108	808.658
	G	809.429	808.742	E1	807.652	807.050
	E2	807.515	806.719	E2	807.701	807.095
	E4	807.579	806.834	E3	805.916	805.227
				E4	805.970	805.333
2 0 1	A1	823.691	824.164	A1	819.009	819.193
	G	822.370	822.840	E1	818.451	818.710
	E1	821.995	822.630	E2	818.364	818.633
	E3	821.689	822.259	E3	818.138	818.488
				E4	817.920	818.254
Unlabeled energy levels		⋮	⋮		⋮	⋮
0 2 1[d]	A1	858.148	860.357	A1	855.085	858.393
	G	857.950	860.106	E1	854.896	858.156
	E1	857.832	859.899	E2	854.913	858.173
	E3	857.778	859.845	E3	854.795	857.961
				E4	854.746	857.914

Notes.
[a] Calculated with the adjusted Hamiltonian of Villa et al. (2011).
[b] Calculated with the refined Hamiltonian of this work.
[c] Calculated with the adjusted Hamiltonian of Carvajal et al. (2012).
[d] Tentative label.

Table 2
Experimental and Calculated Wavenumbers (cm^{-1}) of the Raman Transitions of DME and ^{13}C-DME

Band #	$(v_{11}\ v_{15}\ v_7)_i \rightarrow (v_{11}\ v_{15}\ v_7)_f$	Symm.	$^{12}CH_3O^{12}CH_3$		Symm.	$^{13}CH_3O^{12}CH_3$	
			Calc.[a]	Exp.[b]		Calc.[a]	Exp.[b]
1	0 0 0 → 1 0 0	A3	198.34	197.8 ± 0.2	A2	197.36	···
		G	198.33		E1	197.35	
		E2	198.32		E2	197.35	
		E3	198.32		E3	197.34	
					E4	197.34	
2	0 0 0 → 0 1 0	A2	242.60	241.4 ± 0.4	A2	242.69	241.4 ± 0.5
		G	242.59		E1	242.68	
		E1	242.58		E2	242.68	
		E4	242.58		E3	242.67	
					E4	242.67	
3	0 0 0 → 2 0 0	A1	386.53	385.2 ± 0.2	A1	384.83	385.0 ± 0.2
		G	386.66		E1	384.95	
		E1	386.79		E2	384.96	
		E3	386.79		E3	385.08	
					E4	385.08	
4	1 0 0 → 3 0 0	A3	365.79	362.6 ± 0.2	A2	364.68	362.3 ± 0.2
		G	364.28		E1	363.30	
		E2	363.03		E2	363.24	
		E3	363.03		E3	362.08	
					E4	362.08	
5	0 0 1 → 2 0 1	A1	411.12	411.1 ± 0.2	A1	408.76	409.3 ± 0.2
		G	409.80		E1	408.28	
		E1	409.59		E2	408.20	
		E3	409.22		E3	408.06	
					E4	407.83	
6	0 0 0 → 0 2 0	A1	481.94	482.0 ± 0.2	A1	481.65	481.1 ± 0.2
		G	482.02		E1	481.73	
		E1	482.10		E2	481.73	
		E3	482.10		E3	481.81	
					E4	481.81	
7	1 0 0 → 1 2 0	A3	449.10	450.2 ± 0.4	A2	448.36	449.2 ± 0.5
		G	447.85		E1	447.08	
		E2	446.57		E2	447.12	
		E3	446.56		E3	445.80	
					E4	445.79	
8	0 1 0 → 0 3 0	A2	476.18	480.7 ± 0.2	A2	475.46	479.0 ± 0.3
		G	475.53		E1	474.81	
		E1	474.13		E2	474.81	
		E4	475.09		E3	473.22	
					E4	474.37	
9	0 0 0 → 0 0 1	A1	413.04	412.5 ± 0.2	A1	410.43	410.0 ± 0.2
		G	413.04		E1	410.43	
		E1	413.04		E2	410.43	
		E3	413.04		E3	410.43	
					E4	410.43	
10	1 0 0 → 1 0 1	A3	413.23	413.2 ± 0.2	A2	410.88	410.8 ± 0.2
		G	413.28		E1	410.93	
		E2	413.32		E2	410.94	
		E3	413.32		E3	410.99	
					E4	410.99	
11	0 1 0 → 0 1 1	A2	395.65	395.5 ± 0.2	A2	394.13	393.9 ± 0.2
		G	395.72		E1	394.19	
		E1	395.79		E2	394.19	
		E4	395.79		E3	394.26	
					E4	394.26	
12	2 0 0 → 0 0 2	A1	420.07	424.2 ± 0.2	A1	417.28	422.0 ± 0.3

Table 2
(Continued)

Band #	$(v_{11}\ v_{15}\ v_7)_i \rightarrow (v_{11}\ v_{15}\ v_7)_f$	Symm.	$^{12}CH_3O^{12}CH_3$		Symm.	$^{13}CH_3O^{12}CH_3$	
			Calc.[a]	Exp.[b]		Calc.[a]	Exp.[b]
		G	420.17		E1	417.64	
		E1	420.31		E2	417.61	
		E3	420.18		E3	418.00	
					E4	417.88	
13	2 0 0 → 2 0 1	A1	437.64	437.5 ± 0.5	A1	434.36	434.0 ± 0.2
		G	436.18		E1	433.76	
		E1	435.84		E2	433.68	
		E3	435.47		E3	433.41	
					E4	433.17	
14	0 0 1 → 0 0 2	A1	393.56	396.3 ± 0.3	A1	391.68	394.7 ± 0.2
		G	393.79		E1	392.16	
		E1	394.06		E2	392.13	
		E3	393.93		E3	392.66	
					E4	392.53	
15	0 2 0 → 0 2 1[c]	A1	378.42	381.0 ± 0.2	A1	376.74	379.2 ± 0.2
		G	378.09		E1	376.42	
		E1	377.80		E2	376.44	
		E3	377.75		E3	376.15	
					E4	376.10	

Notes.
[a] Calculated with the refined Hamiltonian of this work.
[b] Experimental.
[c] Tentative assignment.

ν_{11} and ν_{15} bands, had to be forced and strongly modified to reproduce the old data.

Here, with the new Raman reassignments, the discrepancies between experimental and ab initio values decrease significantly: $\Delta = 385.2 - 388.61 = -3.41\text{cm}^{-1}$ for $2\nu_{11}$ and $\Delta = 482.0 - 487.22 = -5.22\ \text{cm}^{-1}$ for $2\nu_{15}$. Thus, both overtones appear now at higher frequencies in the calculations, and gaps between torsional levels are described correctly without any refinement of the B_{011} parameter.

(iii) To reproduce the newly assigned experimental bands, just a few parameters of the Hamiltonian need to be optimized: one kinetic parameter and two potential parameters. In Table 3, the fitted effective potential coefficients (A_{200}, A_{020}) are indicated.

The new optimized Hamiltonians are more confidently used in the assignments of other bands of the two isotopologues and in future works. For example, the IR-forbidden torsional fundamental ν_{11} of DME, calculated ab initio at 199.16 cm^{-1}, is predicted now at 198.33 cm^{-1}, which is much closer to the present experimental observation at 197.8 cm^{-1} (see Figure 2).

Table 1 lists the torsional-bending energies for DME and ^{13}C-DME up to ∼860 cm^{-1} calculated in this work and compares with those reported previously. It should be stressed that the calculated energy levels could be labeled within a $(v_{11}\ v_{15}\ v_7)$ scheme up to ∼825 cm^{-1}, as listed in Table 1. For higher energies, the large torsional splittings and mixing of the wavefunctions impedes the unambiguous assignment of such a $(v_{11}\ v_{15}\ v_7)$ label to all of the computed levels, especially for the less symmetric ^{13}C-DME. The experimental Raman transition wavenumbers of DME and ^{13}C-DME, and their assignments, are listed in Table 2 to facilitate the understanding of Figures 1 and 2, along with the calculated wavenumbers from the fitted energies of Table 1.

5. Concluding Remarks

The spectrum of DME and isotopologues in the THz region is rather complex due to the high density of states, the torsional splittings, the coupling of the torsional overtones with the COC-bending mode, and the presence of many hot bands. Thus, a conclusive assignment of the far-IR spectrum is greatly facilitated by measurements at different temperatures to distinguish between cold and hot bands. This is one of the main results of the present work.

New laboratory measurements of the torsional Raman spectrum of DME and ^{13}C-DME, from room temperature down to 56 K, are reported. This has allowed us to observe the torsional band $\nu_{11} = 197.8\ \text{cm}^{-1}$, which was not reported to date and to reassign its overtone at $2\nu_{11} = 385.2$ and 385.0 cm^{-1} for DME and ^{13}C-DME, respectively. In due turn, this has also allowed us to assign all of the lowest energy levels correctly (see Table 1), which are those relevant for the analysis of the astronomical observations.

The new Raman measurements have been interpreted with the help of highly correlated ab initio calculations within a 3D torsional-vibrational model. The ab initio parameters of the 3D Hamiltonian have been refined using the new experimental data. In the past, such refinement highlighted some problems derived from the lack of experimental data corresponding to the ν_{11} torsional mode, and the large density of states in the region of the torsional overtones, where the coupling with the COC bending occur. These problems have been fixed here, reaching a better agreement with the experiment. Eventually, the quantitative interpretation of the energy level structure in molecules with such large amplitude internal motions must rely on quantum chemical calculations validated by laboratory data.

Table 3
Expansion Coefficients for the Refined CCSD(T)/aug-cc-pVTZ Effective Potential Energy Surface of $^{12}CH_3O^{12}CH_3$ and $^{13}CH_3O^{12}CH_3$

	$^{12}CH_3O^{12}CH_3$	$^{13}CH_3O^{12}CH_3$
Coeff.[a]	V^{eff} [b]	V^{eff} [b]
A_{000}	970.1546	970.1576
A_{100}	−54.6202	−54.7897
A_{200}	10.2064^{fitted}	10.2329^{fitted}
A_{300}	−0.1424	−0.1402
A_{010}	−495.2177	−497.1729
A_{110}	31.7310	31.7310
A_{210}	−1.0805	−1.0805
A_{310}	0.0134	0.0134
A_{011}	25.4803	26.7661
A_{111}	−12.7102	−12.7102
A_{211}	0.5208	0.5208
A_{311}	−0.0056	−0.0056
A_{020}	-1.8845^{fitted}	-0.9984^{fitted}
A_{120}	1.1183	1.1183
A_{220}	−0.1071	−0.1071
A_{320}	0.0038	0.0038
A_{021}	0.7500	0.8149
A_{121}	−0.3289	−0.3289
A_{221}	0.0481	0.0481
A_{321}	−0.0026	−0.0026
A_{022}	1.7800	1.3639
A_{122}	−0.0958	−0.0958
A_{222}	−0.0293	−0.0293
A_{322}	0.0026	0.0026
B_{011}	−13.9554	−15.8995
B_{111}	14.3670	14.3670
B_{211}	−0.7375	−0.7375
B_{311}	0.0117	0.0117

Notes.
[a] Expansion coefficients A_{lmn} and B_{lmn} (in units of $cm^{-1}/degrees^{l}$) of Equation (3).
[b] Refined effective potential parameters. Fitted parameters are indicated.

DME has been observed in excited torsional states in hot astrophysical environments. The present results can help to the characterization of low energy states that can be responsible for unidentified lines of astrophysical surveys, where the presence of the low energy overtones can be relevant. The best-fit Hamiltonian reported here can be used to verify former spectral analyses in the gas phase, and to predict other yet unobserved bands, for future astrophysical detections of other isotopologues of DME in the ISM.

This research is supported by the Spanish Ministerio de Economía y Competitividad (MINECO) under Grants FIS2014-53448-C2-2-P, FIS2016-76418-P and FIS2017-84391-C2, and is partially financed by the Spanish Junta de Andalucía and the European Regional Development Fund (ERDF) under Grant SOMM17/6105/UGR. The authors also acknowledge the European COST Actions CM1401 "Our Astrochemical History" and CM1405 "MOLIM" and CTI (CSIC) and CESGA for computing facilities. Thanks are due to Pia Kutzer and Thomas Giesen (Universität Kassel) for providing the sample of $^{13}CH_3OCH_3$ used in this work.

ORCID iDs

J. M. Fernández https://orcid.org/0000-0002-6636-7978
G. Tejeda https://orcid.org/0000-0003-0810-9652
M. Carvajal https://orcid.org/0000-0001-8743-129X
M. L. Senent https://orcid.org/0000-0003-1878-7377

References

Balucani, N., Ceccarelli, C., & Taquet, V. 2015, MNRAS, 449, L16
Bisschop, S. E., Schilke, P., Wyrowski, F., et al. 2013, A&A, 552, 122
Blukis, U., Kasai, P. H., & Myers, R. J. 1963, JChPh, 38, 2753
Brouillet, N., Despois, D., Baudry, A., et al. 2013, A&A, 550, 46
Bunker, P. R., & Jensen, P. 1989, Molecular Symmetry and Spectroscopy (Ottawa: NRC Research Press)
Carvajal, M., Álvarez-Bajo, O., Senent, M. L., Domínguez-Gómez, R., & Villa, M. 2012, JMoSp, 279, 3
Carvajal, M., Kleiner, I., & Demaison, J. 2010, ApJS, 190, 315
Carvajal, M., Senent, M. L., Villa, M., & Domínguez-Gómez, R. 2014, CPL, 592, 200
Compton, D. A. C., Montero, S., & Murphy, W. F 1980, JPhCh, 84, 3587
Coudert, L. H., Çarçabal, P., Chevalier, M., et al. 2002, JMoSp, 212, 203
Durig, J. R., Li, Y. S., & Groner, P. 1976, JMoSp, 62, 159
Endres, C. P., Drouin, B. J., Pearson, J. C., et al. 2009, A&A, 504, 635
Engeln, R., & Reuss, J. 1991, CP, 156, 215
Engeln, R., Reuss, J., Consalvo, D., et al. 1990, CP, 144, 81
Fantoni, R., van Helvoort, K., Knippers, W., & Reuss, J. 1986, CP, 110, 1
Fateley, W. G., & Miller, F. A. 1962, AcSpe, 18, 977
Favre, C., Carvajal, M., Field, D., et al. 2014, ApJS, 215, 25
Fernández-Sánchez, J. M., Valdenebro, A. G., & Montero, S. 1989, JChPh, 91, 3327
Frisch, M. J., Trucks, G. W., Schlegel, H. B., et al. 2009, Gaussian 09, Revision A.1 (Wallingford, CT: Gaussian, Inc.)
Groner, P., Albert, S., Herbst, E., & de Lucia, F. C. 1998, ApJ, 500, 1059
Groner, P., & Durig, J. R. 1977, JChPh, 66, 1856
Kasai, P. H., & Myers, R. J. 1959, JChPh, 30, 1096
Koerber, M., Bisschop, S. E., Endres, C. P., et al. 2013, A&A, 558, 112
Kutzer, P., Weismann, D., Wassmuth, B., et al. 2016, JMoSp, 329, 28
Lovas, F. J., Lutz, H., & Dreizler, H. 1979, JPCRD, 8, 1051
Neustock, W., Guarnieri, A., Demaison, J., & Wlodarzak, G. 1990, ZNatA, 45, 702
Niide, Y., & Hayashi, M. 2003, JMoSp, 220, 65
Pople, J. A., Head-Gordon, M., & Raghavachari, K. 1987, JChPh, 87, 5968
Richard, C., Margulès, L., Caux, E., et al. 2013, A&A, 552, 117
Schilke, P., Bendford, D. J., Hunter, T. R., Lis, D. C., & Phillips, T. G. 2001, ApJS, 132, 281
Scuseria, G. E., & Schaefer, H. F., III 1989, JChPh, 90, 3700
Senent, M. L. 1998a, JMoSp, 191, 265
Senent, M. L. 1998b, CPL, 296, 299
Senent, M. L. 2001, ENEDIM, A Variational Code for Non-rigid Molecules, http://tct1.iem.csic.es/PROGRAMAS.htm#ENEDIM
Senent, M. L., Domínguez-Gómez, R., Carvajal, M., & Villa, M. 2012, JPCA, 116, 6901
Senent, M. L., Moule, D. C., & Smeyers, Y. G. 1995a, CaJPh, 73, 425
Senent, M. L., Moule, D. C., & Smeyers, Y. G. 1995b, JChPh, 102, 5952
Smeyers, Y. G., Villa, M., & Senent, M. L. 1996, JMoSp, 177, 66
Snyder, L. E., Buhl, D., Schwartz, P. R., et al. 1974, ApJ, 191, L79
Taylor, R. C., & Vidale, G. L. 1957, JChPh, 26, 122
Villa, M., Senent, M. L., & Carvajal, M. 2013, PCCP, 15, 10258
Villa, M., Senent, M. L., Domínguez-Gómez, R., Álvarez-Bajo, O., & Carvajal, M. 2011, JPCA, 115, 13573
Western, C. M. 2016, JQSRT, 186, 221
Woon, D. E., & Dunning, T. H., Jr. 1993, JChPh, 98, 1358